Photocatalytic production of H2 is a multi-criteria optimization problem: case study of RuS2/TiO2

C. Maheu, Eric Puzenat, Pavel Afanasiev, Luis Cardenas, Christophe Geantet

Photocatalytic production of H_2 is a multi-criteria optimization problem: case study of RuS_2/TiO_2

Clément Maheu*, Eric Puzenat, Pavel Afanasiev, Luis Cardenas, Christophe Geantet*

Univ Lyon, Université Claude Bernard Lyon 1, CNRS, IRCELYON, F-69626, Villeurbanne, France

E-mail: christophe.geantet@ircelyon.univ-lyon1.fr
maheu.clement@gmail.com

Abstract

Many parameters influence the photocatalytic production of H_2. Identifying and quantifying them is necessary for correct comparison of photocatalysts and right understanding of involved mechanism.

In this work, we studied the photocatalytic dehydrogenation of isopropanol with titania-supported ruthenium disulfide. We studied the influence of seven parameters on the photocatalytic activity: the temperature, the composition of the reactive mixture, the mass of the photocatalyst, the flux and the energy of the incident photons, the co-catalyst loading and the nature of the support. Their influence was studied, not only on the rate of hydrogen production (or photon yield) but also on the apparent activation energy and on the pre-exponential factor, deduced from an Arrhenius law.

The photon yield as a function of the co-catalyst loading show an optimum of activity. A 6.9 % photon yield was obtained at 0.84 wt% and $E_{photons} = 3.65\ eV$.

The rate-determining step for the photocatalytic dehydrogenation of the isopropanol with RuS_2/TiO_2 is, at optimal conditions, the electron transfer from TiO_2 to RuS_2. The latter is not favored because of the band diagrams of RuS_2 and TiO_2. The electron transfer can be optimized working with incident photons having a higher energy, thanks to a hot carrier effect observed in RuS_2/TiO_2.

Keywords

Photocatalytic hydrogen evolution reaction; Ruthenium disulfide; Titanium dioxide; Co-catalyst; Activation energy; UPS analysis.

Table of content

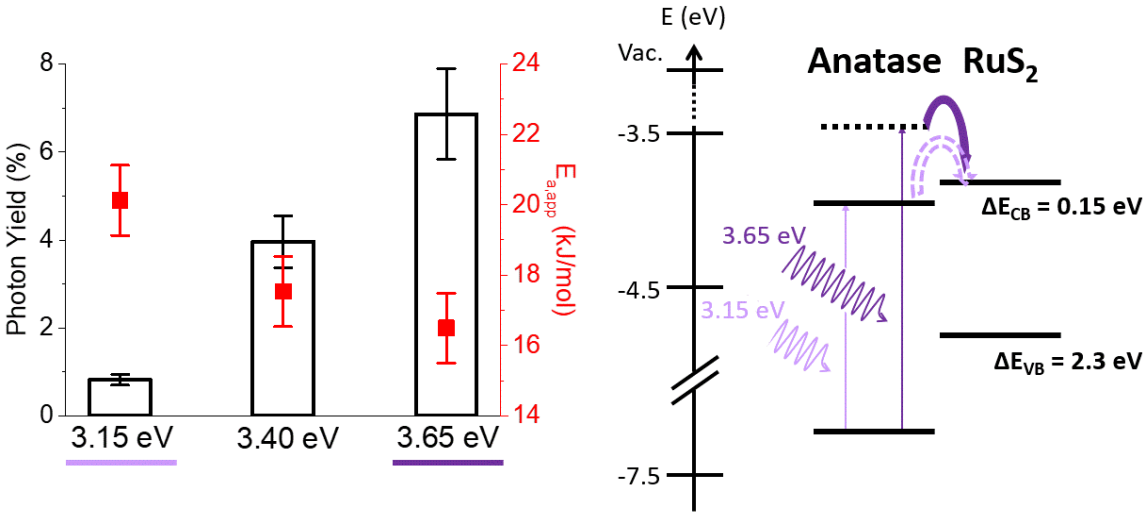

Introduction

Photocatalysis is a promising strategy providing green and renewable source of energies. Photocatalysis of endergonic reactions, such as artificial photosynthesis, would store solar energy, an abundant but intermittent source of energy, in the form of chemical energy (*i.e. solar fuels*) [1,2]. Photocatalytic production of H_2, a promising vector of energy, could allow renewable process using water and/or bio-based alcohols as a feedstock.

Jaramillo and coll., calculated that a single bed particle suspension can reach a solar to hydrogen efficiency of 11.2 % and produce one kg of H_2 for $1.60 [3]. However, such efficiency was never reached. Addition of a co-catalyst to a light absorbing semiconductor enhance the charge carriers separation and their utilization [4]. The resulting rate for the photocatalytic hydrogen evolution reaction (PHER) is therefore increased. Several noble metal co-catalysts were reported in the literature (with Pt, the most studied) [5–12] as well as oxides [13–15] or transition metal sulfides co-catalysts [16–24]. However, no photocatalytic system is efficient enough to produce sustainable H_2 at a reasonable cost. Intense current research efforts are directed to the design of efficient co-catalysts.

Numerous current empirical studies focus on novel co-catalysts without providing mechanistic insights. An important issue is to compare photocatalytic efficiency measured in different laboratories. Indeed the conditions of the experiments strongly varied and many parameters influence the PHER rate. It depends, for instance on the incident flux of photons, the mass of photocatalyst or the reactive mixture [25–28]. Without identifying and quantifying those parameters, it is impossible to provide accurate comparison from one photocatalyst to another. Herein to conduct such a detailed study, we use the photocatalytic dehydrogenation of the isopropanol as a model reaction and the titania-supported ruthenium disulfide as a model photocatalyst.

The photocatalytic dehydrogenation of the isopropanol is proposed as a model reaction. It mimics the production of clean and renewable H_2 with raw biomass, the targeted feedstock. Promising work has been done on carbohydrates [29], on polysaccharides [30], on crude glycerol [31] and more recently on unprocessed biomass by Reisner and co-workers (for instance, grass, rice or seaweeds) [32–34]. However, for more fundamental studies, mono-alcohol systems are preferred. The PHER rate and the observed rankings of co-catalysts performance strongly depend on the nature of the alcohol [5,6,8,17,35]. We proposed the photocatalytic conversion of a water-isopropanol mixture for its simplicity, as it proceeds via a single dehydrogenation pathway.

Titania-supported ruthenium disulfide (RuS_2/TiO_2) is proposed as a model photocatalyst. Since the discovery of its photocatalytic activity [2,36], TiO_2 is by far the most studied photocatalyst [4,37]. By contrast, RuS_2 is not the most studied transition metal sulfide

co-catalyst. More attention has been recently paid to MoS_2 [20,21,38–40], to NiS_x [23,41,42] or to cheaper materials such as CuS [24,43]. However, we recently evidenced that among a series of seven transition metal sulfides deposited on TiO_2, RuS_2 was one of the most efficient PHER co-catalyst [17].

RuS_2 is a well-known hydrodesulfurization catalyst [44–47]. It has also been reported for photoelectrocatalytic applications [48–51] and a few times for PHER. RuS_2 has been reported as a co-catalyst of TiO_2 [22], TiO_2-SiO_2 [52] and $Cd_xZn_{1-x}S$ [53] but also as a photocatalyst itself. RuS_2 particles were reported on SiO_2 or on thiol-modified polystyrene particles [22,54,55]. In the S.I., the activities of these RuS_2-based photocatalysts are reported (See Table S1). However, the diversity of the reactive mixture in which the materials are studied forbids an accurate comparison.

This work aims to evaluate the influence of seven of the crucial reaction parameters that influence the PHER rate: the temperature, the concentration of isopropanol, the mass of photocatalyst, the nature of the TiO_2 support, the RuS_2 loading, the energy and the flux of the incident photons. The influence of some of those parameters on the PHER rate were already quantified. However, to provide better insight into the mechanism we study not only PHER rates but also, two kinetic parameters derived from the Arrhenius law: an apparent activation energy ($E_{a,app}$) and a pre-exponential factor (A_{app}).

1. Experimental

2.1 Materials and catalyst preparation

The RuS_2-based photocatalysts were prepared with the thioacetamide reflux method. Details on the synthesis and on the characterization were reported previously [17,38]. Typically, 2.0 g of commercial TiO_2 (CristalACTIV^{TM} PC500) (referred latter as PC500) and 900 mg of thioacetamide (Alfa Aesar) were suspended in 100 mL of deionized water. Suspension was refluxed under stirring prior to introduce the precursor salt: $RuCl_3.xH_2O$ (Sigma Aldrich). The amount of precursor varied to obtain several co-catalyst loadings. The solid materials were isolated by centrifugation, washed and dried under N_2. Bulk RuS_2 sample were prepared in the same conditions, for characterization.

A second preparation method consisted in mechanically mixing the bulk RuS_2 with five titania supports: PC500 (anatase), a homemade rutile [56], a homemade brookite [57] and two commercial mixed phase titania from Evonik Aeroxide®: P25 (80/20 wt%, anatase / rutile) and Aeroxide® P90 (92/8 wt%, anatase / rutile), referred latter as P90 and P25.

2.2 Characterization of the catalysts

Temperature-programmed reduction (TPR) was carried out in a quartz reactor from room temperature to 1050 °C at a rate of 5 °C.min^{-1}. The samples (50–100 mg) were heated under H_2 flow (50 ml min^{-1}). A Thermo Prolab quadrupole mass-spectrometer detected the H_2S produced.

X-ray diffraction (XRD) patterns were obtained using a Bruker D8 Advance A25 diffractometer equipped with a Ni filter (with Cu-K_α, radiation 0.154184 nm) and a 1-dimensional multistrip detector (Lynxeye, 192 channels on 2.95°). Diffractogram were analyzed with Diffrac.Eva software using standard JCPDS files for phase identification.

Transmission electron microscopy (TEM) was carried out on a JEOL 2010 LaB_6 device with an accelerating voltage 200 keV. Its point to point resolution is 0.19 nm. The apparatus is equipped with an Energy-dispersive X-ray spectroscopy (EDX) analyzer (Link ISIS – Oxford Instrument). The annular-dark-field STEM experiments (ADF-STEM) were performed with a FEI Titan ETEM G2 electron microscope equipped with a Cs image aberration corrector and operated at 300 keV. The extraction voltage, camera length, acceptance angles, STEM resolution and probe current were 4500 V, 245 mm, 29.2–146°, 0.14 nm and < 0.1 nA, respectively. For sample preparation, the powder was sonicated in ethanol and dropped onto a TEM grid. To protect them from air oxidation, samples were immediately introduced into the TEM vacuum chamber.

The metal content in the synthesized solids was determined, after dissolution in an acid mixture, by inductively coupled plasma optical emission spectrometry (ICP-OES Activa

Jobin Yvon). For Ru-based materials a dissolution in H_2SO_4, HNO_3 and HF under 150 °C during one night was employed. Elemental analysis of light elements (CHNS) was also performed on an analyzer Thermo Fisher Flash 2000.

Textural properties were studied by N_2 adsorption-desorption isotherms. BET surface areas (S_{BET}) were determined using a multipoint BET method. The measurements were carried out using N_2 adsorption-desorption at −196 °C in a Micromeritics ASAP 2020 device. Before S_{BET} analysis, the catalyst samples were degassed at 250 °C under vacuum (10^{-6} bar) for 3 h.

To prepare the electrodes, 20 mg of photocatalytic nanopowders were dispersed by ultrasound in 800 µL of ethanol. The resulting suspension was drop-casted on a FTO glass substrate (7 $\Omega.cm^{-2}$, purchased from Sigma-Aldrich). The electrodes were characterized through electrochemical impedance spectroscopy (EIS). A three-electrode electrochemical cell was used with Pt wire as counter electrode and an SCE (3 M KCl) as reference electrode. The electrolyte is a 0.1 M $KClO_4$ solution with a pH 8. The impedance spectra were recorded on a VMP300, Biologic potentiostat with the Software EC-Lab, between 100 mHz and 200 kHz with 12 points per decade, 2 measures per frequency and an amplitude of 100 µA.

Photoelectron spectroscopy measurements were conducted in an integrated ultrahigh vacuum system: Axis Ultra DLD system Kratos Analytical. X-ray photoelectron spectroscopy (XPS) analysis was performed with a monochromatized Al K_α X-ray source (1486.6 eV). XPS spectra were acquired at 160 eV and 40 eV of pass energy for low and high resolution respectively. The wide spectrum (from 1200 to -5 eV) was recorded in order to identify all chemical species on the surface. High resolution core-level spectra were recorded at dwell time of 200 ms and a step of 0.1 eV. Number of scans varies to limit the signal-to-noise ratio. The photon source power was fixed at 15 mA and 15 kV. Data were analyzed with CasaXPS software. The binding energy (BE) of all electronic states were referenced to the C 1s main state at 284.5 eV; this energy position was assigned to C-C or C-H bonds. A Shirley background was then subtracted to the spectra. Core level such as, C 1s, O 1s or S 2p were decomposed into a combination of Voigt functions. For specific core levels such as Ru 3d, an asymmetric line shape was used: a product of a Doniach Sunjich with a Gaussian/Lorentzian function.

2.3 UPS and Diffuse Reflectance Spectroscopy

Ultraviolet photoelectron spectroscopy (UPS) analysis is widely used for electronic structure characterisation, ultraviolet light increase the detection sensitivity concomitant with

the high photoionization cross-sections in the valence band region [58]. We have developed a methodology to study nanopowders by UPS [59,60].

UPS spectra were acquired using a He I ($h\nu = 21.2$ eV) resonant line. High resolution UPS spectrum was obtained by using a spatial lens aperture of 110 µm and 10 eV of pass energy. Under these conditions, the intrinsic resolution of the spectra was estimated about 0.2 eV with the method reported by Schlaf *et al.* [61] and Reinert *et al.* [58] (See Figure S1). In contrast, XPS analysis is less sensitive to valence band analysis. However, this type of XPS measurements can provides a general information about the electronic structure of the system, despite its low resolution (around 0.5 eV, see Figure S1 for determination).

Powder samples were ultrasonically dispersed in pentane, and, deposited on a conducting substrate by a drop-casting method. Drop-casting was made on ITO substrate for valence band (VB) states identification (*i.e.* experimental density of states (DOS)) and on an Ag foil for absolute band diagram determination. UPS spectra were subtracted with a Henrich – type background [62].

UV-Visible diffuse reflectance spectroscopy (UV-Vis DRS) was measured at room temperature with a Perkin Elmer Lambda 45 spectrometer. It is equipped with an integrating sphere (RSA-PE-20). Pure $BaSO_4$ (Alfa Aesar, 99%) was used as a reference and to dilute the powders. Kubelka-Munk function (F_{KM}) was applied to represent absorbance. It is valid for the values of reflectance $R_\infty > 0.6$ and therefore several dilution in $BaSO_4$ were performed [63]. The band-gap (E_g) values were estimated from the plot of $((F_{KM}\, h\nu)^{1/n}$ *versus* energy, so-called Tauc plot [64].

2.4 Photocatalytic tests

The photocatalytic set-up is depicted on Figure S2. Photocatalytic reaction was conducted in liquid phase, in a double-wall semi-batch slurry reactor with 600 rpm stirring. The reactor is made of pyrex, its dimensions are provided in Figure S2. The reactor was filled with the RuS_2/TiO_2 photocatalyst slurry in 50 mL of an aqueous solution of isopropanol (Carlo Erba, 99.9 %). It is then sonicated during 10 minutes to obtain a homogeneous slurry. Notice that the isopropanol is put in large excess, the conversion is therefore always below 2 %. The experimental conditions are summarized in Table S2.

Before irradiation, the system was purged with Ar flow (100mL/min) for 30 min. The Ar flow was then decreased to 20mL/min. After checking that the system reached a steady state and that no product is formed under dark conditions, the light was switched on. Gases were analyzed with a micro gas chromatograph (µ-GC) equipped with four columns (Molecular Sieve 5 Å, PPU, Alumina and Wax) and thermal conductivity detectors (Agilent Technologies, 300 A). The rate of hydrogen production (r_{H_2}) was measured after waiting 2 h

that the system reached a steady. The r_{H_2} was calculated from the average concentration of H_2 measured over 1 h.

The reactor has an optical window of 20 cm^2 area. Three lamps were used to illuminate it. The first is a polychromatic 125 W high-pressure mercury lamp (HPK). The second is a monochromatic 370 nm LED (LZ1 BIN N from Engine). Both emit line spectra. The intensity of the LED lamp can be tuned applying different electrical power. The third lamp is a 300 W Xe lamp (MAX-302, Asahi Spectra), which emits continuous spectrum, its intensity and the wavelength range can be tuned using filters. Their respective irradiance spectra were acquired with a radiometer device and are shown in Figure S3 and S4. The glassware of the photoreactor filters the wavelength below 290 nm and the band gap of the TiO_2-PC500 is 3.15 eV [59]; wavelength above 390 nm cannot be absorbed. Therefore, we calculated the incident flux of photons that can be absorbed (290 – 390 nm range): $\Phi_{photons-absorbable}$ (the total incident flux of photons is also provided in the SI).

The photon yield (PY) was calculated as r_{H_2} divided by this $\Phi_{photons-absorbable}$ [65]. Note that in the case of polychromatic irradiation (HPK), PY should be called “photonic efficiency”, in agreement with the IUPAC nomenclature [25,65]. However, for the sake of simplicity, only PY is used herein. The error on the PY was estimated to be close to 10 %.

A cryostat (Julabo Cryostat F32-ME) supplied water recirculation in the double-wall of the reactor to adjust its temperature between 10 and 45 °C. If the opposite is not clearly indicates, the reported r_{H_2} and PY are measured at 20 °C.

2. Results and Discussion

3.1 Characterization of the RuS_2/TiO_2 photocatalyst

XRD pattern of the RuS_2/TiO_2 photocatalyst evidences only the TiO_2 anatase phase (See Figure S5). It is due to the amorphous structure of RuS_x obtained with the thioacetamide reflux method. It confirms that the support does not have any effect on the crystallization of the RuS_x co-catalyst.

XPS measurement was performed to identify the RuS_x state (See Figure S6). Because the Ru 3p signal overlaps with the Ti 2p one and because the Ru 3d 3/2 signal overlaps with the C 1s, it requires a meticulous fit of the XPS spectra. More details on the methodology were provided in [17]. Core level states at 279.9 (Ru 3d – C 1s) and 161.9 eV (S 2p) correspond to the pyrite state $(S\text{-}S)^{2-}$ [66]. XPS spectra also show that the RuS_x phase is not pure, the small contribution at 166-171 eV can be assigned to sulfate groups [67] and the state at BE = 281.0 eV corresponds to a more oxidized RuS_xO_y state. Indeed, no particular cautions were used to avoid air contact prior to the PHER tests or to insertion in the XPS analysis chamber.

XPS analyses were also performed on RuS_2/TiO_2 after being tested for PHER for 20 h (See Figure S7). It evidences that RuS_2 particles are partially oxidized after test. This might be due to the consumption of holes by the RuS_2 instead of isopropanol oxidation. According to the electronic structure that will be discussed at the end, the transfer of holes from TiO_2 to RuS_2 is favorable.

Using STEM analyses, the high mass of Ru relatively to Ti permits easy detection of RuS_2 particles at the surface of TiO_2 (See Figure S8). The size of the particles was therefore estimated between 1 nm and 1.5 nm. As a complementary technic to access RuS_2 particle size, we used TPR measurements.

Several type of sulfur species have been evidenced on the TPR curve of the RuS_2/TiO_2 prepared with the thioacetamide reflux method (See Figure S9). Three types of sulfur were discriminated: the one from thioacetamide impurities ($S_{thio.}$), the one from the sulfur at the surface ($S_{surf.}$), and in the bulk (S_{bulk}). A geometrical model discussed in [68] correlates the ratio $\frac{S_{surf.}}{S_{surf.}+S_{bulk}}$ with the size of particles having a pyrite structure. It estimates an average size of 1.3 ± 0.2 nm for the RuS_2 particles, supported on TiO_2, in agreement with STEM results.

Therefore, the thioacetamide reflux method leads to amorphous RuS_2 particles of 1.3 nm supported on TiO_2.

3.2 Co-catalytic effect of RuS_2 on TiO_2

RuS_2/TiO_2 photocatalysts were then tested for the photocatalytic dehydrogenation of the isopropanol. Three products were detected by µ-GC: acetone, H_2 and propene. The two first products result of a dehydrogenation pathway and the last results of the dehydration of isopropanol:

$$CH_3CHOHCH_3 \rightarrow CH_3COCH_3 + H_2$$

$$CH_3CHOHCH_3 \rightarrow CH_2 = CHCH_3 + H_2O$$

As the rate of hydrogen production is 97 times higher than that of propene production, the dehydration pathway is neglected. No CO_2 was detected, it indicates that the total reforming of the isopropanol or its total oxidation does not occur. The absence of O_2 in the reactor prevent the total oxidation. The unsuitable water:isopropanol stoichiometry prevent the total reforming. A mechanistic and a kinetic study for the dehydrogenation of isopropanol are beyond the scope of this work and will be discussed elsewhere. The PHER rates were measured at 10, 20, 35 and 45 °C for RuS_2/TiO_2 and for bare TiO_2. At each temperature, the RuS_2/TiO_2 was significantly more active than TiO_2. Figure 1 depicts the evolution of the H_2 concentration along the time. The resulting PHER rate and the PY both follow an Arrhenius law. It therefore provides two additional kinetic parameters, a pre-exponential factor (A_{app}) and an apparent activation energy ($E_{a,app}$):

$$PY = \frac{r_{H_2}^{exp}}{\Phi_{photons\ -absorbable}} \times 100 \quad (1)$$

$$PY = \frac{A_{app\ ,r_{H_2}}}{\Phi_{photons\ -absorbable}} e^{\frac{-E_{a,app}}{RT}} = A_{app\ ,PY}.e^{\frac{-E_{a,app}}{RT}}$$

The error on the $E_{a,app}$ was estimated lower than 1.0 kJ/mol by reproducing the experiment three times for some of the catalysts reported in this work.

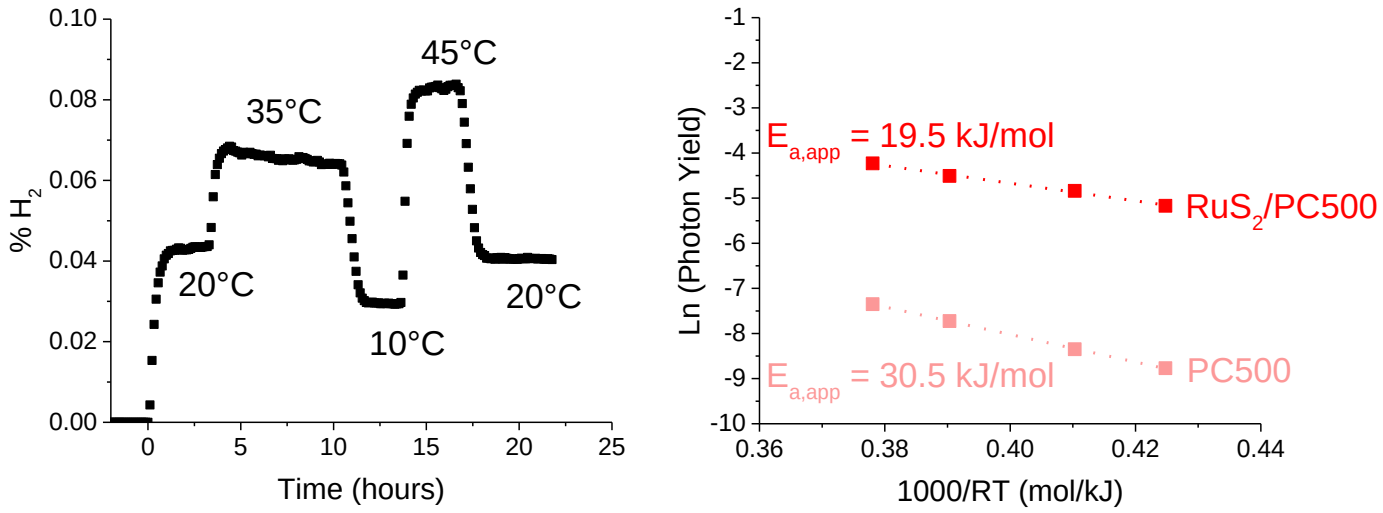

Figure 1: Photocatalytic dehydrogenation of isopropanol (6.5 mol/L) with RuS_2/PC500 (0.73 wt% Ru) (40 mg) (thioacetamide reflux method) ($\Phi_{photons\ -absorbable}$ = 800 µE/h): (left) Molar fraction of H_2 as a function of the time and thus, of the photoreactor temperature; (right) Arrhenius plot for RuS_2/PC500 and bare PC500 with four temperatures: 10, 20, 35 and 45 °C. Slope and intersection with y-axis give $E_{a,app}$ and A_{app}, respectively.

First, the $E_{a,app}$ values were compared for bare PC500 at 30.5 kJ/mol and for RuS_2/PC500 at 19.5 kJ/mol. Deposition of RuS_2 on the TiO_2 surface lowers the apparent activation energy of PHER. It evidences the co-catalytic effect of RuS_2 for two commercial TiO_2 supports (PC500 and P25) (See Figure S10).

The unsupported RuS_2 do not produce H_2 in similar experimental conditions. Therefore, the enhancement factor (*i.e.* $\frac{r_{H_2}(RuS_2/TiO_2)}{r_{H_2}(TiO_2)}$) and the synergetic factor (*i.e.* $\frac{r_{H_2}(RuS_2/TiO_2)}{r_{H_2}(TiO_2)+r_{H_2}(RuS_2)}$) are equal. The measured enhancement factors are 4.1 and 25.9 for P25 and PC500 supports, respectively.

Activation energies are often measured in thermal heterogeneous catalysis but they are rarely reported in photocatalysis. The few values reported in the literature are lower than those related to thermal catalysis and are between 5 and 30 kJ/mol [35,69–72]. For instance Ait-Ichou *et al.* measured an activation energy of 72.4 kJ/mol with Pt/TiO_2 for the dehydrogenation of isopropanol in the dark and of 9.2 kJ/mol under irradiation [69]. In addition, Turek and Krowiak measured the activation energy for the dehydrogenation of the isopropanol with various metal oxides [73]. Values are between 50 kJ/mol and 130 kJ/mol. Therefore it indicates that the presence of light and of a semiconducting material decrease of one order of magnitude the activation energy of the isopropanol dehydrogenation.

Because the PHER occurs near to ambient while for thermal catalysis it starts at 70 °C [69,73], the sensitivity of the PHER rate to $E_{a,app}$ is high for photocatalysis. Small variations of the $E_{a,app}$ value significantly influences the PY. The presence of RuS_2 co-catalyst at the surface of the PC500 surface decreases the $E_{a,app}$ by a factor 1.5 but the exponential term, at 20 °C, increases by a factor 50 (See Figure S11).

Activation energy measurements were performed for the photocatalytic oxidation of alcohols with Pt/TiO_2 [35,69,71] or noble-metal-free TiO_2 [70,72]. Because all the reported $E_{a,app}$ values are generally low, literature works assumed that adsorption, desorption or migration phenomena are the rate-determining steps. Here, for the first time, $E_{a,app}$ is measured for a transition metal sulfide – based catalyst: RuS_2/TiO_2. To understand the physical nature of the rate-determining step, we studied the influence of six parameters on the $E_{a,app}$. It was measured with the same procedure than the one illustrated by Figure 1 (PY is measured during the steady state reach for each of the four temperatures).

The measurement of $E_{a,app}$ and A_{app} provides two additional kinetic parameters. With the PY or the PHER rate, they were used to study the photocatalytic behavior of RuS_2/TiO_2 and to provide mechanistic insights.

3.3 Optimal experimental conditions

Prior to study the influence of the targeted parameters, the optimal experimental conditions were established. The influence of the concentration of alcohol in the reactive mixture, of the photocatalyst mass and of the incident flux of photons were measured on the PHER rate (or PY). It was already analyzed in the literature, for instance by Herrmann [11], but it the first time that the influence of these parameters on the $E_{a,app}$ and A_{app} was investigated.

Between 1.3 mol/L and 13 mol/L of isopropanol, the PHER rate as well as the $E_{a,app}$ does not does not vary significantly (See Figure S12). The apparent kinetic order of isopropanol is consider as 0: $r_{H_2} = k\,.\,[isopropnaol]^0$. We therefore assumed that above 1.3 mol/L the oxidation half-reaction does not limit the overall PHER process. The photocatalytic tests were further conducted in the same 1:1 %vol. mixture of isopropanol and water.

The PHER rate linearly increases with the mass of photocatalyst, until to reach a plateau (See Figure S13). It is a common phenomenon already reported in the literature [11,21,25,74,75]. It is due to the Lambert-Bouger law governing the light absorption of a photocatalyst. Therefore, we proposed to model these data with the following expression:

$$r_{H_2} = r_{H_2,max} \cdot (1 - e^{-\alpha.m}) \quad (2)$$

$r_{H_2,max}$ is the PHER at the plateau, $\alpha(\lambda)$ (g^{-1}) is the absorption coefficient of the photocatalyst and m is its mass.

This model works for PC500, P25 and P90 – based photocatalyst (See Figure S14). Notice that the threshold between the linear and the plateau region of r_{H_2} vs mass of the photocatalyst varies as the function of the titania support. Therefore, it seems mandatory to plot a $r_{H_2} = f(mass_{photocatalyst})$ curve fort reporting the optimal PHER rate of a given photocatalyst.

When the mass of photocatalyst is increased, $E_{a,app}$ slightly decreased until it reached a plateau. Below 40 mg, the limiting irradiated surface area prevents an optimal photon absorption. The limiting amount of charge carriers governs the overall PHER rate. Therefore, the following photocatalytic tests were conducted with at least 40 mg of photocatalyst (See Table S2).

When the mass of photocatalyst increased, $A_{app,PY}$ also decreased until it reached a plateau. We assumed that $A_{app,r_{H_2}}$ depends on the density of photons available per irradiated surface ($\rho_{photons}$):

$$A_{app,r_{H_2}} \propto \rho_{photons} = \frac{\Phi_{photons-absorbable}}{S_{irrad.}} \quad (3)$$

With $S_{irrad.}$, the surface of the irradiated particles.

At a given flux of incident photons, the higher the mass of photocatalyst is, the higher the surface of irradiated particles is, the lower the $\rho_{photons}$ is. The TiO_2 has therefore a lower probability to absorb a photon. The $A_{app,PY}$ therefore decreases until to reach a plateau for which the additional photocatalyst mass is not irradiated.

Finally, the influence of the incident flux of photons ($\Phi_{photons-absorbable}$) was studied. Figure 2 evidences two regimes. At low intensity, the PHER rate evolves linearly with the flux $\Phi_{photons-absorbable}$: the higher the amount of photons is, the higher the amount of free charge carriers is and therefore, the higher the amount of H_2 produced is. At higher intensities, it is no longer the case. The threshold between the two trends is estimated at 2800 ± 200 µEinstein/h (µE/h).

We performed irradiance measurement at different spot of the photoreactor (See Figure S15 for additional details). It confirms that the second regime is not due to photons that are transfered or diffused outside of the photoreactor.

It confirms experimentally the existence of two regimes on a $r_{H_2} = f(\Phi_{photons-absorbable})$ curve that Hermann theorized in [11]. At high intensity, he explained that the charge carrier recombination is predominant. The TiO_2 surface absorbs too many photons, photogenerated charge carriers are not transfered fast enough to the co-catalyst and most of them recombine. He proposed an evolution of the PHER rate, as follows:

$$r_{H_2} = a \,.\, \Phi_{photons-absorbable}{}^{0,5} \quad (4)$$

With a, being a constant. The curve in Figure 2 can be fitted with such expression at high intensity (See Figure S16). This relationship has been already proven experimentally with TiO_2-P25 for the photocatalytic degradation of sulfonylurea herbicides [76] and CdS for the PHER [77]. However, the threshold was reached at different intensities. It shows that this behavior depends on various parameters related to the photocatalytic support, the nature of the co-catalyst and the geometry of the reactor.

As the PHER rate linearly evolves with the lamp intensity, it seems more instructive to report PY. For that purpose, providing the references of the lamp or its power is not enough, its actual intensity depends on the lamp age and on the brand. Therefore, the incident flux of photons must be reported. However, calculating a PY at high intensity underestimates the efficiency of a photocatalyst. Reporting a $r_{H_2} = f(\Phi_{photons-absorbable})$ curve is therefore recommended for any novel photocatalytic set-up and/or material [75].

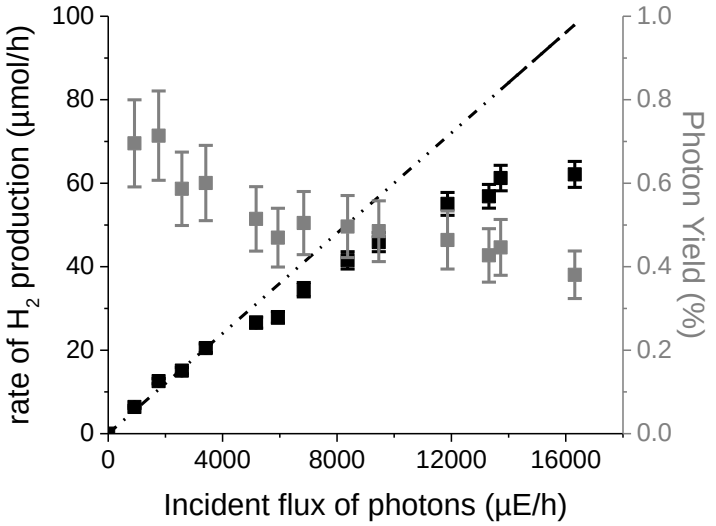

Figure 2: Photocatalytic dehydrogenation of isopropanol (6.5 mol/L) with RuS_2/PC500 (1.15 wt% Ru) (50 mg) (thioacetamide reflux method) as a function of the incident flux of photons that can be absorbed ($\boldsymbol{\Phi_{photons-absorbable}}$). PHER rate (black squares) and photon yield (grey squares) are depicted. Dotted line corresponds to the expected r_{H2} = cte $\boldsymbol{\Phi_{photons-absorbable}}$.

For our photocatalytic set-up, the optimal experimental conditions were established: a 1:1 %vol. mixture of isopropanol and water for not being limited by the oxidation half-reaction, a mass of photocatalyst higher than 40 mg for not being limited by the photon absorption and a well-known and well-controlled incident flux of photons for an accurate comparison of the catalyst. The targeted parameters (the nature of the support, the co-catalyst loading and the energy of the incident photons) can therefore be studied.

3.4 Influence of the titania support

In our previous work [17], seven transition metal sulfides were compared as co-catalysts on the same titania support (PC500). RuS_2 appeared to be one of the best co-catalysts in the series. Therefore, we wanted to compare several semiconducting supports with the same co-catalyst. Here, the same RuS_2 co-catalyst was deposited on five titania materials. Figure 3 shows the PHER activity of the resulting photocatalysts. Among the titania samples, three are pure phases (commercial PC500 anatase, homemade rutile [56] and homemade brookite [57]) and two are mixtures of anatase and rutile phases (P90 and P25).

RuS_2 was first synthesized with the thioacetamide reflux method and then mechanically mixed with TiO_2. It allows avoiding the differences of RuS_2 properties that would probably appear, if it were chemically grown on different titania materials. Mechanical mixing guarantees uniformity of RuS_2 properties and allows focusing on the differences between TiO_2 samples. The amorphous structure of the bulk RuS_x evidenced with XRD (See Figure S5) confirm that the RuS_2 particles has size of few nanometers, as the one obtained with the thioacetamide reflux method.

A comparison with the standard thioacetamide reflux method shows that this preparation method does not significantly influence the photocatalytic activity (See Figure S17). One explanation could be that the sonication used before each photocatalytic test to homogenize the slurry (See Section 2.4) has a benefic effect on the slurry. A second one would be that the direction formation of the RuS_2 particles at the surface of the TiO_2, with the thioacetamide reflux method, does not provide a better intimacy than the mechanical mixture of pre-synthesized RuS_2 and TiO_2. Another explanation would be that RuS_2 particles might not need to be in a close contact with the titania surface during the all photocatalytic process. Afanasiev, recently evidenced that TiO2 particles can accumulate long-live photogenerated charge carriers until a contact with a co-catalyst particle occurs. Active catalysts could be obtained without close intimacy [78].

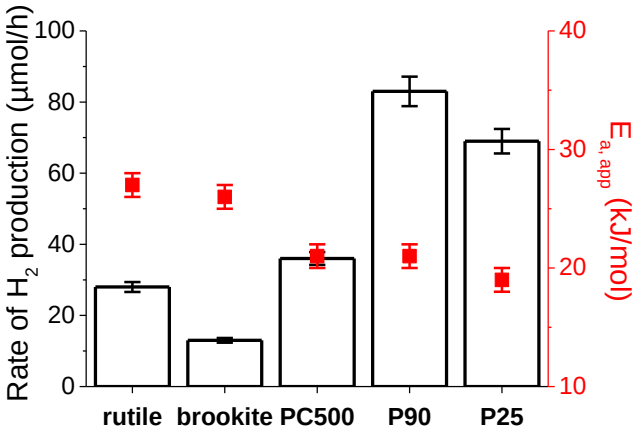

Figure 3: Photocatalytic dehydrogenation of isopropanol (6.5 mol/L) with RuS_2/PC500 (0.4 wt% Ru) (50 mg) (mechanical mixture followed by sonication) ($\Phi_{photons\ -absorbable}$ = 6000 µE/h) as a function of the titania support. Photon yield (black bar charts) and $E_{a,app}$ (red squares) are depicted.

The PHER rates vary as a function of the titania sample. In average, the mixed phases are more active than the pure phases. For the latter, the ranking is: brookite < rutile < anatase. Several parameters can influence the PHER rates vs. the nature of titania samples [4,79]. First, they have various surface areas that influence the amount of adsorption sites. The amount of photons absorbed depends on the surface surface of the irradiated particle and also on the band gap of the semiconductors. The morphology of photocatalytic powders (agglomeration, shape of crystallites) also has an influence, as well as their crystallinity. Finally, the position of the valence band defines the potential of the photogenerated holes and therefore its capacity to oxidize isopropanol.

The $E_{a,app}$ values vary as a function of the titania material. It suggests that the rate-determining step does not involve processes occurring merely on the RuS_2 co-catalyst. Low $E_{a,app}$ values observed in the literature, led the authors to conclude that desorption of H_2 or H^+ migration should be the rate-determining step [70,72]. The results presented in Figure 3 go against such hypotheses because H^+ species are reduced and H_2 is formed on the same RuS_2 co-catalyst, used in all five compositions. On the other hand for the previously studied series of MS_x supported on the same TiO_2 [17] (and many literature works dealing with the PHER co-catalysts design) a strong dependence of PHER rate on the nature of co-catalyst evidences that the photocatalytic H_2 production cannot be defined by the intrinsic properties of the TiO_2 itself. Therefore, the rate-determining step probably involves both the RuS_2 and the TiO_2. We believe that such a rate-determining step is either the electron transfer from the TiO_2 to the RuS_2 or the charge carrier separation, occurring on the TiO_2 but enhanced with

the presence of a co-catalyst. In both cases, the amount of TiO_2-RuS_2 interface must influence the PHER activity of the resulting heterostructure. To explore this hypothesis, the co-catalyst loading was varied and its influence on the kinetic parameters was measured.

3.5 Influence of the RuS_2 loading

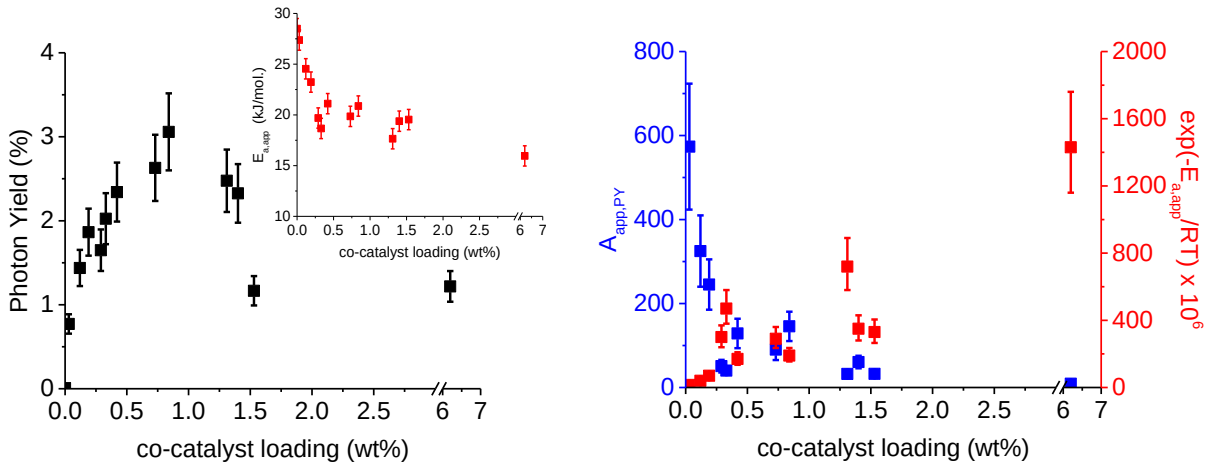

Figure 4: Photocatalytic dehydrogenation of isopropanol (6.5 mol/L) with RuS_2/PC500 (50 mg) (thioacetamide reflux method) ($\Phi_{photons\ -absorbable}$ = 800 µE/h) as a function of the co-catalyst loading. Photon yield (black squares) and $E_{a,app}$ (red squares) are depicted on the left, as well as the $A_{app\ ,PY}$ (blue squares) and the $e^{-\frac{E_{a,app}}{RT}}$ (red squares) on the right.

Figure 4 reports the PHER rate as a function of RuS_2 loading. It has maximal values in the range of 0.5-1 wt%. At low co-catalyst loadings, the activity increases until the amount of co-catalyst becomes sufficient. For the high loadings, the PHER rate decreased above 1% wt. (See Figure 4, left). In the region of optimal mass loadings of RuS_2, the PHER rate has a plateau or a smooth maximum.

The highest PY of 3.1 % is obtained for 0.84 wt% loading. It can be noted that the optimization of the co-catalyst loading improved the PY by a factor 1.6 (from 1.9 % to 3.1 %), in comparison to our previous work [17] (See Table S1). In the S.I. the activity of MS_x-based photocatalysts are reported: their yield, as well as their enhancement factors (*i.e.* the ratio of the rates of hydrogen production with and without the co-catalyst). The diversity of the reactive mixture prevents a comparison with the RuS_2-based photocatalysts. However, comparison with other co-catalysts from the literature shows a reasonably high activity (See Table S1). The RuS_2/TiO_2 photocatalyst has a higher enhancement factor than CuS [24,43] and NiS – based catalyst [41,42]. It is even competitive with MoS_2 – based materials [38,39]. The highest yield and the highest enhancement factor are however measured with amorphous MoS_X co-catalyst [21,40].

From bare titania to highly loaded RuS_2/TiO_2 the activation energy progressively decreased approximately twice, from ca. 30 to ca. 15 KJ/mol (Figure 4, inset). It suggests

that the rate-determining step is gradually favored with the increase of the co-catalyst loading. To explore one hypothesis, we performed EIS experiments on the RuS_2-based photocatalysts (See Figure S18). In dark conditions, it shows a progressive increase of the conductivity with the increase of the co-catalyst loading. It might be due to an enhanced electron transfer between the TiO_2 and the RuS_2

The decrease of the $E_{a,app}$ with an increase of the co-catalyst loading is however compensated by also a decrease of the pre-exponential part in the PHER rate expression (See Figure 4, right). This compensation leads to the appearance of the PY optimum

On bare TiO_2 or at low RuS_2 loading, hydrogen is released on many sites corresponding to the high TiO_2 surface but with relatively high activation energy (probably that of hydrogen atoms recombination). When more RuS_2 is added, H_2 is predominantly formed on fewer sites located on the sulfide and with low activation energy that corresponds to a process involving the co-catalyst (which cannot be identified exactly and might correspond to the charge carriers behavior, as discussed previously).

The decrease of PHER rate at high co-catalyst loading might be explained by different causes, from light absorption by the (black) co-catalyst to the agglomeration of co-catalyst particles and decrease of their efficiency. Such behavior of PHER rate vs. the co-catalyst loading is well known in the literature for different systems, but not fully understood [23,41,53,80].

We observe that the increase of the co-catalyst loading does not significantly modify the morphology of the RuS_2 particles. Their size always remains within the range 1-1.5 nm (See Figure S8). Therefore, deterioration of the co-catalyst properties seems less probable. Otherwise the negative effect of high loadings is often explained in the literature by shielding effect of the co-catalyst [10,53,80–82]. Without dismissing the data of these works, we exclude this hypothesis in our case. Indeed, bare PC500 has a BET surface area of 276 m^2/g, the loading of 1.5 wt% Ru decreases the BET surface area to 269 m^2/g. It corresponds to approximately one RuS_2 particle of 1.2 nm size per 20 nm^2 of titania, which can hardly be considered as shielding.

The decrease of PHER activity in methanol on Pt and Pd -loaded TiO_2 was previously attributed to the overlapping of surface zones where the particles provide optimal electrons harvesting. As far as such zones begin to overlap, the conditions deteriorate in the overlapping areas, as the electronic properties of TiO_2 are somehow unfavorably modified [83].

To explain decrease of PHER rate at relatively low co-catalyst loadings, we suppose that the PHER rate might be limited by the relatively high recombination rate of electron–hole pairs. Previously the possibility has been demonstrated for electrons and holes to be recombined on the same co-catalyst sink [84,85]. Simulation of rate processes is beyond the

scope of this work, but the effects might be explained in qualitative terms. If the co-catalyst is efficient not only for electrons harvesting but also for the electron-hole pairs recombination, then at too high concentration of RuS_2 sites on the surface, electrons and holes might mostly recombine on the sulfide before being used for the reaction.

To confirm such hypothesis and to discuss the electron transfers between the TiO_2 and the RuS_2, the electronic structure of the heterostructure was determined.

3.6 Electron transfer and influence of the incident photons energy

The methodology proposed in [59], combining UPS and UV-Vis DRS describes the electronic structure of RuS_2/TiO_2. First, UPS measurements were performed on bare TiO_2 (PC500), bulk RuS_2 and RuS_2/TiO_2. The sample prepared on an ITO substrate gives VB states identification and a sample prepared on an Ag foil gives the absolute position of the E_{VB}. Dropping a low quantity of diluted slurry on Ag allows obtaining an UPS spectrum with the contributions of both the sample powder and the Ag foil (See Figure S19 and S20). The Fermi step of the Ag is used as an internal standard calibration for the spectra. The E_{VB} are therefore positioned on an absolute scale at: -7.1 eV for TiO_2 (PC500) [59] and -4.8 eV for both bulk RuS_2 and RuS_2/TiO_2 (See Figure 5). The E_{VB} of bulk and supported RuS_2 are the same. It means that when the E_F of TiO_2 and RuS_2 are aligned, the E_{VB} of RuS_2 is not modified. It concludes that E_F of TiO_2 and of RuS_2 are close.

After an appropriate background subtraction, it is possible to curve fit the experimental DOS of RuS_2/TiO_2. It was represented as a superposition of Voigt functions corresponding to individual states. The same states as for bare TiO_2 are needed for fitting RuS_2/TiO_2, as well as one additional component, assigned to a RuS_2 state. To confirm such hypothesis, UPS spectrum of a more concentrated sample (6.2 wt% Ru) was acquired. Indeed, the higher the RuS_2 loading is, the more intense this state is (See Figure S21). It corresponds probably to the Ru 4d t_{2g} orbitals (brown curve at the highest energy on Figure 5) [86]. The other states on the UPS spectrum of bulk RuS_2 correspond to the hybridized Ru 4d e_g – S 3p orbitals.

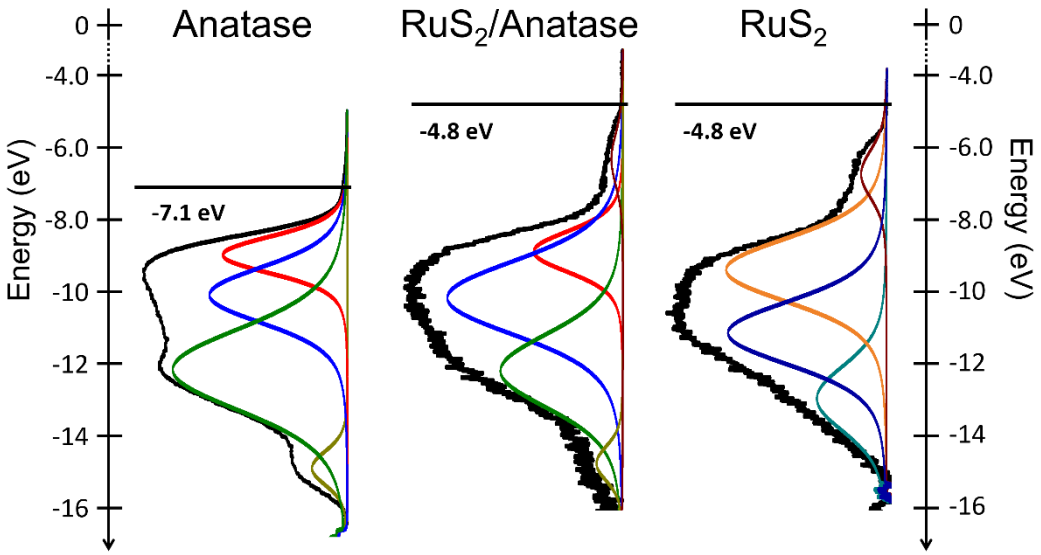

Figure 5: UPS spectra of bare TiO_2 (PC500), of RuS_2/TiO_2 and bulk RuS_2.

UV-Vis DRS was performed on bulk RuS_2 and RuS_2/TiO_2. It shows an indirect band gap of 1.0 eV for RuS_2 (See Figure S22 and S23). A direct transition is also observed at 1.9 eV. Those results agree with the literature [87,88]. At 1.4 eV a transition is also observed, it is assigned to an excitonic peak; a particular state near the valence maximum, photoexcited to the conduction band of RuS_2.

Using E_g = 1.0 eV, the E_{CB} of RuS_2 is deduced at -3.8 eV. It is 0.15 eV closer to the vacuum level than the one of TiO_2-PC500 (-3.95 eV [59]). It agrees with the band diagram proposed by Hara *et al.* (except that they report a much larger band gap) [22]. The electron transfer from TiO_2 to RuS_2 is therefore not favored. As these energy levels are measured in particular conditions (under ultra high vacuum), Mott Schotky analysis would be interested to perform since the presence of an electrolyte can mimic the wet conditions used of a photocatalytic test [78].

To go further in the investigation of this electron transfer, photocatalytic tests were performed at three energies of the incident photons ($E_{photons}$). Figure 6 displays the measured PY (*i.e.* so-called action spectra), the $E_{a,app}$ and the $A_{app\ ,PY}$.

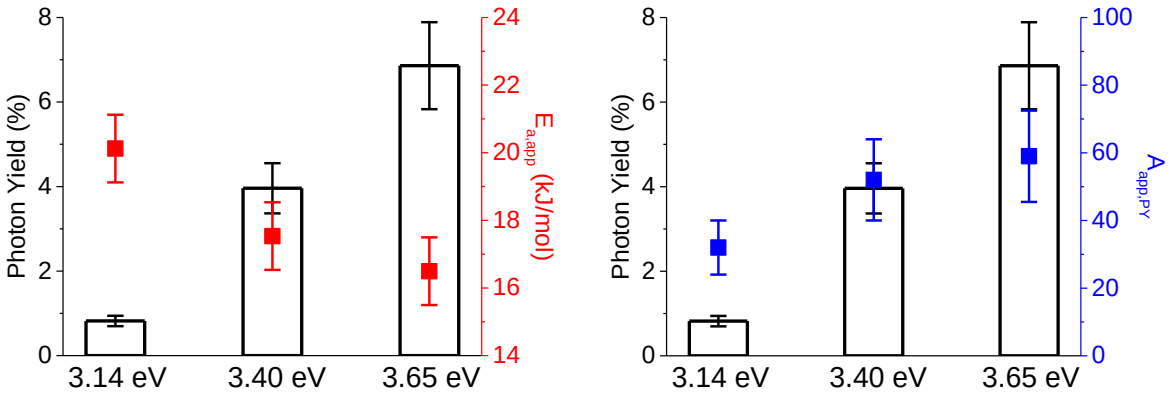

Figure 6: Photocatalytic dehydrogenation of isopropanol (6.5 mol/L) with RuS_2/PC500 (0.84 wt% Ru) (40 mg) (thioacetamide reflux method) as a function of the energy of the incident photons. The later was tuned, applying different filters to the Xe lamp. Photon yield (black bar charts), $E_{a,app}$ (red squares) and $A_{app\,,PY}$ (blue squares) are depicted.

The PY increases as a function of $E_{photons}$. It can be due to an intrinsic effect of the $E_{photons}$ and/or to the absorption properties of the RuS_2/TiO_2 photocatalyst. Indeed, the absorption coefficient of the photocatalyst increases as a function of $E_{photons}$: $\alpha_{TiO_2}(3.65\,eV) \approx 10\,\alpha_{TiO_2}(3.4\,eV) \approx 250\,\alpha_{TiO_2}(3.14\,eV)$ (See Figure S22). The higher the amount of photons absorbable by TiO_2 is the higher the number of photogenerated charge carriers is and therefore the higher PHER rate is.

The evolution of the $E_{a,app}$ values as a function of $E_{photons}$ evidences an intrinsic effect of the photons energy. The rate-determining step is influenced by $E_{photons}$; photons with an energy of 3.65 eV are more efficient than those with an energy of 3.14 eV. We assigned this phenomenon to a favorable transfer of the electrons for $E_{photons}$ = 3.65 eV (See Scheme 1). At $E_{photons} = 3.14\,eV$, photons have only enough energy to be excited from the top of the VB to the bottom of the CB. Only few electrons could be transfered to RuS_2 and are responsible of the co-catalytic effect of RuS_2 ($E_{a,app}$ (RuS_2/TiO_2) < $E_{a,app}$ (TiO_2)). At $E_{photons} = 3.65\,eV$, the same top VB states are excited to higher CB states and can be easily transfered from TiO_2 to RuS_2. This transfer occurs only if the additional kinetic energy is not lost due to thermalization. The latter is a phenomenon occurring at the femtosecond scale [89] while the electron transfer occurs at the picosecond scale [90]. These results therefore suggest a hot carrier effect in the RuS_2/TiO_2 photocatalyst where the thermalization is delayed of few order of magnitude. The hot electrons are then transfered to RuS_2 and the

favorable transfer decreases the $E_{a,app}$ measured. It is not the first time that hot charge carriers were evidenced in photocatalysts [91,92].

To confirm the presence of hot electrons and to investigate the electronic transfer additional characterization can be considered, such as time-resolved photoluminescence [93].

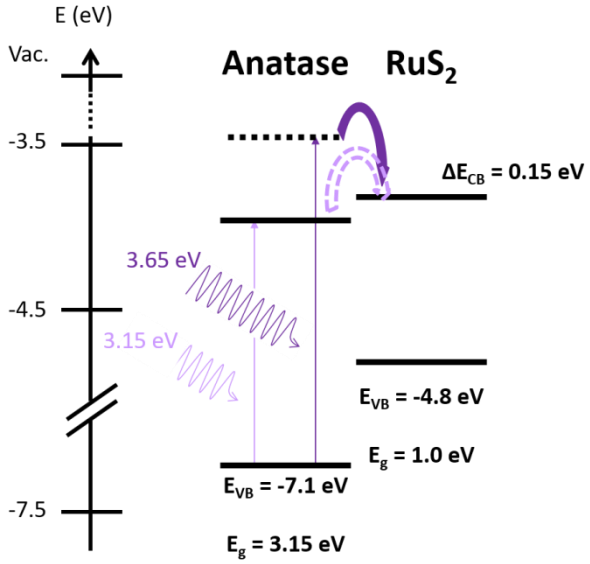

Scheme 1: Hot carrier effect in the RuS_2/TiO_2 photocatalyst

The PY increases due to a lower $E_{a,app}$ but also due to a higher $A_{app\ ,PY}$ for higher $E_{photons}$ (See Figure 5). We explained the increasing $A_{app\ ,PY}$ by its dependence on the amount of active sites: $(RuS_{2,surf}\ ; e^-)$. In a classic heterogeneous catalytic process, the activity depends on the amount of $RuS_{2,surf}$ sites available. In photocatalysis, these sites participate to the H_2 formation only if they have received an electron from TiO_2 to reduce H^+. The number of $(RuS_{2,surf}\ ; e^-)$ depends therefore on the morphology of the photocatalyst but also on the behaviour of the photogenerated electrons. With a higher $E_{photons}$, electrons can not only be excited from a given VB state to higher CB states but also, higher $E_{photons}$ can excite deeper VB states. It results that more VB states are excited therefore more electrons transfer and the amount of $(RuS_{2,surf}\ ; e^-)$ increases.

3. Conclusion

This work provides a detailed study of the influence of several essential parameters on the PHER performance of RuS_2/TiO_2 photocatalyst for the dehydrogenation of the isopropanol. Temperature, flux and energy of the incident photons, alcohol concentration, photocatalyst mass, nature of the titania support and co-catalyst loading were varied. Their influence was coherently explained.

The influence of these parameters was not only studied on the PY but also on two additional kinetic parameters: $E_{a,app}$, A_{app} . It is the first time that these parameters are used to investigate a photocatalytic mechanism.

The PHER system contains several functional elements. Concerted functioning of these elements is necessary to provide optimal PHER performance, from light absorption to hydrogen atoms recombination on the co-catalyst. The single rate-limiting step of PHER does not exist, as depending on the conditions any of the steps might become the bottleneck one. Thus, at low content of organic substrate, holes accommodation and concomitant charges separation might become limiting or when the co-catalyst is lacking or deficient, hydrogen release and/or electron transfer are probably limiting..

The experimental conditions (*i.e.* concentration of isopropanol, mass of the photocatalyst, flux of photons, co-catalyst loading) were optimized. The highest photon yield of this work was obtained for a 0.84 wt% RuS_2 loading on anatase TiO_2; PY = 3.1 % with the HPK lamp and PY = 6.9 % with the Xe lamp combined with a filter centered at 3.65 eV.

As shows the analysis of PY, $E_{a,app}$ and A_{app} , under optimal conditions the slow reaction step is probably related to charge separation processes. Indeed the full band diagram of the RuS_2/TiO_2 photocatalyst shows an unfavored electron transfer from TiO_2 to RuS_2. It seems however that the delayed thermalization of the charge carriers and their excess of kinetic energy permits this transfer and therefore, the production of H_2 at the surface of the RuS_2/TiO_2 co-catalyst.

Conflicts of interest

The authors declare no competing financial interest.

Acknowledgments

C. M. acknowledges financial support from the French Ministry of Education. C. M. also acknowledges the DivCat of the *Société Chimique de France* for its grant to participate to the MACS VIII.

References

[1] A.J. Bard, Photoelectrochemistry and heterogeneous photo-catalysis at semiconductors, Journal of Photochemistry. 10 (1979) 59–75. https://doi.org/10.1016/0047-2670(79)80037-4.
[2] S.J. Teichner, The origins of photocatalysis, Journal of Porous Materials. 15 (2008) 311–314. https://doi.org/10.1007/s10934-006-9091-1.
[3] B.A. Pinaud, J.D. Benck, L.C. Seitz, A.J. Forman, Z. Chen, T.G. Deutsch, B.D. James, K.N. Baum, G.N. Baum, S. Ardo, H. Wang, E. Miller, T.F. Jaramillo, Technical and economic feasibility of centralized facilities for solar hydrogen production via photocatalysis and photoelectrochemistry, Energy & Environmental Science. 6 (2013) 1983. https://doi.org/10.1039/c3ee40831k.
[4] J. Schneider, M. Matsuoka, M. Takeuchi, J. Zhang, Y. Horiuchi, M. Anpo, D.W. Bahnemann, Understanding TiO_2 Photocatalysis: Mechanisms and Materials, Chemical Reviews. 114 (2014) 9919–9986. https://doi.org/10.1021/cr5001892.
[5] H. Bahruji, M. Bowker, P.R. Davies, F. Pedrono, New insights into the mechanism of photocatalytic reforming on Pd/TiO_2, Applied Catalysis B: Environmental. 107 (2011) 205–209. https://doi.org/10.1016/j.apcatb.2011.07.015.
[6] M. Bowker, C. Morton, J. Kennedy, H. Bahruji, J. Greves, W. Jones, P.R. Davies, C. Brookes, P.P. Wells, N. Dimitratos, Hydrogen production by photoreforming of biofuels using Au, Pd and Au–Pd/TiO_2 photocatalysts, Journal of Catalysis. 310 (2014) 10–15. https://doi.org/10.1016/j.jcat.2013.04.005.
[7] G.L. Chiarello, M.H. Aguirre, E. Selli, Hydrogen production by photocatalytic steam reforming of methanol on noble metal-modified TiO_2, Journal of Catalysis. 273 (2010) 182–190. https://doi.org/10.1016/j.jcat.2010.05.012.
[8] Z.H.N. Al-Azri, W.-T. Chen, A. Chan, V. Jovic, T. Ina, H. Idriss, G.I.N. Waterhouse, The roles of metal co-catalysts and reaction media in photocatalytic hydrogen production: Performance evaluation of M/TiO_2 photocatalysts (M = Pd, Pt, Au) in different alcohol–water mixtures, Journal of Catalysis. 329 (2015) 355–367. https://doi.org/10.1016/j.jcat.2015.06.005.
[9] C. Dessal, L. Martínez, C. Maheu, T. Len, F. Morfin, J.L. Rousset, E. Puzenat, P. Afanasiev, M. Aouine, L. Soler, J. Llorca, L. Piccolo, Influence of Pt particle size and reaction phase on the photocatalytic performances of ultradispersed Pt/TiO2 catalysts for hydrogen evolution, Journal of Catalysis. 375 (2019) 155–163. https://doi.org/10.1016/j.jcat.2019.05.033.

[10] T.A. Kandiel, A.A. Ismail, D.W. Bahnemann, Mesoporous TiO_2 nanostructures: a route to minimize Pt loading on titania photocatalysts for hydrogen production, Phys. Chem. Chem. Phys. 13 (2011) 20155. https://doi.org/10.1039/c1cp22612f.
[11] J.-M. Herrmann, Heterogeneous photocatalysis: state of the art and present applications., Topics in Catalysis. 34 (2005) 49–65. https://doi.org/10.1007/s11244-005-3788-2.
[12] G. Jeantelot, M. Qureshi, M. Harb, S. Ould-Chikh, D. H. Anjum, E. Abou-Hamad, A. Aguilar-Tapia, J.-L. Hazemann, K. Takanabe, J.-M. Basset, TiO_2-supported Pt single atoms by surface organometallic chemistry for photocatalytic hydrogen evolution, Physical Chemistry Chemical Physics. 21 (2019) 24429–24440. https://doi.org/10.1039/C9CP04470A.
[13] A.S. Hainer, J.S. Hodgins, V. Sandre, M. Vallieres, A.E. Lanterna, J.C. Scaiano, Photocatalytic Hydrogen Generation Using Metal-Decorated TiO_2: Sacrificial Donors vs True Water Splitting, ACS Energy Letters. 3 (2018) 542–545. https://doi.org/10.1021/acsenergylett.8b00152.
[14] J. Sato, N. Saito, Y. Yamada, K. Maeda, T. Takata, J.N. Kondo, M. Hara, H. Kobayashi, K. Domen, Y. Inoue, RuO_2-Loaded β-Ge_3N_4 as a Non-Oxide Photocatalyst for Overall Water Splitting, J. Am. Chem. Soc. 127 (2005) 4150–4151. https://doi.org/10.1021/ja042973v.
[15] M. Higashi, R. Abe, A. Ishikawa, T. Takata, B. Ohtani, K. Domen, Z-scheme Overall Water Splitting on Modified-TaON Photocatalysts under Visible Light (λ<500 nm), Chem. Lett. 37 (2007) 138–139. https://doi.org/10.1246/cl.2008.138.
[16] L. Zheng, F. Teng, X. Ye, H. Zheng, X. Fang, Photo/Electrochemical Applications of Metal Sulfide/TiO_2 Heterostructures, Advanced Energy Materials. (2019). https://doi.org/10.1002/aenm.201902355.
[17] C. Maheu, E. Puzenat, C. Geantet, L. Cardenas, P. Afanasiev, Titania - Supported transition metals sulfides as photocatalysts for hydrogen production from propan-2-ol and methanol, International Journal of Hydrogen Energy. 44 (2019) 18038–18049. https://doi.org/10.1016/j.ijhydene.2019.05.080.
[18] S. Shen, X. Chen, F. Ren, C.X. Kronawitter, S.S. Mao, L. Guo, Solar light driven photocatalytic hydrogen evolution over $ZnIn_2S_4$ loaded with transition-metal sulfides, Nanoscale Research Letters. 6 (2011) 1–6. https://doi.org/10.1186/1556-276X-6-290.
[19] M. Tabata, K. Maeda, T. Ishihara, T. Minegishi, T. Takata, K. Domen, Photocatalytic hydrogen evolution from water using copper gallium sulfide under visible-light irradiation, The Journal of Physical Chemistry C. 114 (2010) 11215–11220. https://doi.org/10.1021/jp103158f.
[20] B. Chen, Y. Meng, J. Sha, C. Zhong, W. Hu, N. Zhao, Preparation of MoS_2/TiO_2 based nanocomposites for photocatalysis and rechargeable batteries: progress, challenges, and perspective, Nanoscale. 10 (2018) 34–68. https://doi.org/10.1039/C7NR07366F.
[21] K. Chang, H. Pang, X. Hai, G. Zhao, H. Zhang, L. Shi, F. Ichihara, J. Ye, Ultra-small freestanding amorphous molybdenum sulfide colloidal nanodots for highly efficient photocatalytic hydrogen evolution reaction, Applied Catalysis B: Environmental. 232 (2018) 446–453. https://doi.org/10.1016/j.apcatb.2018.03.087.
[22] K. Hara, K. Sayama, H. Arakawa, Photocatalytic hydrogen and oxygen formation over SiO_2-supported RuS_2 in the presence of sacrificial donor and acceptor, Applied Catalysis A: General. 189 (1999) 127–137. https://doi.org/10.1016/S0926-860X(99)00260-4.
[23] F. Xu, L. Zhang, B. Cheng, J. Yu, Direct Z-Scheme TiO_2/NiS Core–Shell Hybrid Nanofibers with Enhanced Photocatalytic H_2-Production Activity, ACS Sustainable Chem. Eng. 6 (2018) 12291–12298. https://doi.org/10.1021/acssuschemeng.8b02710.
[24] Q. Wang, N. An, Y. Bai, H. Hang, J. Li, X. Lu, Y. Liu, F. Wang, Z. Li, Z. Lei, High photocatalytic hydrogen production from methanol aqueous solution using the photocatalysts CuS/TiO_2, International Journal of Hydrogen Energy. 38 (2013) 10739–10745. https://doi.org/10.1016/j.ijhydene.2013.02.131.

[25] M. Qureshi, K. Takanabe, Insights on Measuring and Reporting Heterogeneous Photocatalysis: Efficiency Definitions and Setup Examples, Chemistry of Materials. 29 (2017) 158–167. https://doi.org/10.1021/acs.chemmater.6b02907.
[26] T. Le Bahers, K. Takanabe, Combined theoretical and experimental characterizations of semiconductors for photoelectrocatalytic applications, Journal of Photochemistry and Photobiology C: Photochemistry Reviews. (2019). https://doi.org/10.1016/j.jphotochemrev.2019.01.001.
[27] P.V. Kamat, S. Jin, Semiconductor Photocatalysis: "*Tell Us the Complete Story!*," ACS Energy Letters. 3 (2018) 622–623. https://doi.org/10.1021/acsenergylett.8b00196.
[28] J. Schneider, D.W. Bahnemann, Undesired Role of Sacrificial Reagents in Photocatalysis, The Journal of Physical Chemistry Letters. 4 (2013) 3479–3483. https://doi.org/10.1021/jz4018199.
[29] T. Kawai, T. Sakata, Conversion of carbohydrate into hydrogen fuel by a photocatalytic process, Nature. 286 (1980) 474. https://doi.org/10.1038/286474a0.
[30] D.I. Kondarides, V.M. Daskalaki, A. Patsoura, X.E. Verykios, Hydrogen Production by Photo-Induced Reforming of Biomass Components and Derivatives at Ambient Conditions, Catalysis Letters. 122 (2008) 26–32. https://doi.org/10.1007/s10562-007-9330-3.
[31] P. Ribao, M. Alexandra Esteves, V.R. Fernandes, M.J. Rivero, C.M. Rangel, I. Ortiz, Challenges arising from the use of TiO_2/rGO/Pt photocatalysts to produce hydrogen from crude glycerol compared to synthetic glycerol, International Journal of Hydrogen Energy. (2018). https://doi.org/10.1016/j.ijhydene.2018.09.148.
[32] D.W. Wakerley, M.F. Kuehnel, K.L. Orchard, K.H. Ly, T.E. Rosser, E. Reisner, Solar-driven reforming of lignocellulose to H_2 with a CdS/CdO_x photocatalyst, Nature Energy. 2 (2017) 17021. https://doi.org/10.1038/nenergy.2017.21.
[33] M.F. Kuehnel, E. Reisner, Solar Hydrogen Generation from Lignocellulose, Angewandte Chemie International Edition. 57 (2018) 3290–3296. https://doi.org/10.1002/anie.201710133.
[34] H. Kasap, D.S. Achilleos, A. Huang, E. Reisner, Photoreforming of Lignocellulose into H_2 Using Nanoengineered Carbon Nitride under Benign Conditions, Journal of the American Chemical Society. 140 (2018) 11604–11607. https://doi.org/10.1021/jacs.8b07853.
[35] Y. Yang, C. Chang, H. Idriss, Photo-catalytic production of hydrogen form ethanol over M/TiO_2 catalysts (M=Pd, Pt or Rh), Applied Catalysis B: Environmental. 67 (2006) 217–222. https://doi.org/10.1016/j.apcatb.2006.05.007.
[36] N. Serpone, A.V. Emeline, S. Horikoshi, V.N. Kuznetsov, V.K. Ryabchuk, On the genesis of heterogeneous photocatalysis: a brief historical perspective in the period 1910 to the mid-1980s, Photochemical & Photobiological Sciences. 11 (2012) 1121. https://doi.org/10.1039/c2pp25026h.
[37] Y. Ma, X. Wang, Y. Jia, X. Chen, H. Han, C. Li, Titanium Dioxide-Based Nanomaterials for Photocatalytic Fuel Generations, Chemical Reviews. 114 (2014) 9987–10043. https://doi.org/10.1021/cr500008u.
[38] E. Girel, E. Puzenat, C. Geantet, P. Afanasiev, On the photocatalytic and electrocatalytic hydrogen evolution performance of molybdenum sulfide supported on TiO_2, Catalysis Today. 292 (2017) 154–163. https://doi.org/10.1016/j.cattod.2016.09.018.
[39] Y.-J. Yuan, Z.-J. Ye, H.-W. Lu, B. Hu, Y.-H. Li, D.-Q. Chen, J.-S. Zhong, Z.-T. Yu, Z.-G. Zou, Constructing Anatase TiO_2 Nanosheets with Exposed (001) Facets/Layered MoS_2 Two-Dimensional Nanojunctions for Enhanced Solar Hydrogen Generation, ACS Catal. 6 (2016) 532–541. https://doi.org/10.1021/acscatal.5b02036.
[40] F. Du, H. Lu, S. Lu, J. Wang, Y. Xiao, W. Xue, S. Cao, Photodeposition of amorphous MoS_x cocatalyst on TiO_2 nanosheets with {001} facets exposed for highly efficient photocatalytic hydrogen evolution, International Journal of Hydrogen Energy. 43 (2018) 3223–3234. https://doi.org/10.1016/j.ijhydene.2017.12.181.
[41] J. Huang, Z. Shi, X. Dong, Nickel sulfide modified TiO_2 nanotubes with highly efficient photocatalytic H_2 evolution activity, Journal of Energy Chemistry. 25 (2016) 136–140. https://doi.org/10.1016/j.jechem.2015.11.007.

[42] Y. Xin, Y. Lu, C. Han, L. Ge, P. Qiu, Y. Li, S. Fang, Novel NiS cocatalyst decorating ultrathin 2D TiO_2 nanosheets with enhanced photocatalytic hydrogen evolution activity, Materials Research Bulletin. 87 (2017) 123–129. https://doi.org/10.1016/j.materresbull.2016.11.027.
[43] K. Manjunath, V.S. Souza, G. Nagaraju, J. Marcos Leite Santos, J. Dupont, T. Ramakrishnappa, Superior activity of the CuS–TiO_2/Pt hybrid nanostructure towards visible light induced hydrogen production, New J. Chem. 40 (2016) 10172–10180. https://doi.org/10.1039/C6NJ02241C.
[44] T.A. Pecoraro, R.R. Chianelli, Hydrodesulfurization catalysis by transition metal sulfides, Journal of Catalysis. 67 (1981) 430–445. https://doi.org/10.1016/0021-9517(81)90303-1.
[45] C.J.H. Jacobsen, E. Törnqvist, H. Topsøe, HDS, HDN and HYD activities and temperature-programmed reduction of unsupported transition metal sulfides, Catalysis Letters. 63 (1999) 179–183. https://doi.org/10.1023/A:1019017004845.
[46] M. Lacroix, N. Boutarfa, C. Guillard, M. Vrinat, M. Breysse, Hydrogenating properties of unsupported transition metal sulphides, Journal of Catalysis. 120 (1989) 473–477. https://doi.org/10.1016/0021-9517(89)90287-X.
[47] J.A. De Los Reyes, Ruthenium sulfide supported on alumina as hydrotreating catalyst, Applied Catalysis A: General. 322 (2007) 106–112. https://doi.org/10.1016/j.apcata.2007.01.004.
[48] A. Kratzig, C. Zachäus, S. Brunken, D. Thomas, P. Bogdanoff, K. Ellmer, S. Fiechter, RuS_2 thin films as oxygen-evolving electrocatalyst: Highly oriented growth on single-crystal FeS_2 substrate and their properties compared to polycrystalline layers: RuS_2 thin films as oxygen-evolving electrocatalyst, Physica Status Solidi (a). 211 (2014) 2020–2029. https://doi.org/10.1002/pssa.201431284.
[49] H. Ezzaouia, R. Heindl, R. Parsons, H. Tributsch, Visible Light Photo-oxidation of water with single-crystal, J. Electroanal. Chem. 145 (1983) 279–292. https://doi.org/10.1016/S0022-0728(83)80087-4.
[50] M. Ashokkumar, A. Kudo, N. Saito, T. Sakata, Semiconductor sensitization by RuS_2 colloids on TiO_2 electrodes, Chemical Physics Letters. 229 (1994) 383–388. https://doi.org/10.1016/0009-2614(94)01098-6.
[51] S. Licht, S. Ghosh, H. Tributsch, S. Fiechter, High efficiency solar energy water splitting to generate hydrogen fuel: Probing RuS_2 enhancement of multiple band electrolysis, Solar Energy Materials and Solar Cells. 70 (2002) 471–480. https://doi.org/10.1016/S0927-0248(01)00041-1.
[52] T.-V. Nguyen, S. Kim, O.-B. Yang, Water decomposition on TiO_2–SiO_2 and RuS_2/TiO_2–SiO_2 photocatalysts: the effect of electronic characteristics, Catalysis Communications. 5 (2004) 59–62. https://doi.org/10.1016/j.catcom.2003.11.007.
[53] A.P. Gaikwad, D. Tyagi, C.A. Betty, R. Sasikala, Photocatalytic and photo electrochemical properties of cadmium zinc sulfide solid solution in the presence of Pt and RuS_2 dual co-catalysts, Applied Catalysis A: General. 517 (2016) 91–99. https://doi.org/10.1016/j.apcata.2016.03.006.
[54] K. Hara, K. Sayama, H. Arakawa, Photocatalytic Activity of RuS_2/SiO_2 for Water Decomposition, Chemistry Letters. (1998) 387–388. https://doi.org/10.1246/cl.1998.387.
[55] T. Hirai, Y. Nomura, I. Komasawa, Immobilization of RuS_2 Nanoparticles Prepared in Reverse Micellar System onto Thiol-Modified Polystyrene Particles and their Photocatalytic Properties, Journal of Nanoparticle Research. 5 (2003) 61–67. https://doi.org/10.1023/A:1024422226598.
[56] H. Li, P. Afanasiev, On the selective growth of titania polymorphs in acidic aqueous medium, Materials Research Bulletin. 46 (2011) 2506–2514. https://doi.org/10.1016/j.materresbull.2011.08.023.
[57] H. Li, M. Vrinat, G. Berhault, D. Li, H. Nie, P. Afanasiev, Hydrothermal synthesis and acidity characterization of TiO_2 polymorphs, Materials Research Bulletin. 48 (2013) 3374–3382. https://doi.org/10.1016/j.materresbull.2013.05.017.

[58] F. Reinert, S. Hüfner, Photoemission spectroscopy-from early days to recent applications, New Journal of Physics. 7 (2005) 1–34. https://doi.org/10.1088/1367-2630/7/1/097.
[59] C. Maheu, L. Cardenas, E. Puzenat, P. Afanasiev, C. Geantet, UPS and UV spectroscopies combined to position the energy levels of TiO_2 anatase and rutile nanopowders, Physical Chemistry Chemical Physics. 20 (2018) 25629–25637. https://doi.org/10.1039/C8CP04614J.
[60] C. Larquet, A.-M. Nguyen, E. Glais, L. Paulatto, C. Sassoye, M. Selmane, P. Lecante, C. Maheu, C. Geantet, L. Cardenas, C. Chanéac, A. Gauzzi, C. Sanchez, S. Carenco, Bandgap Engineering from Cation Balance: the Case of Lanthanide Oxysulfide Nanoparticles, Chem. Mater. (2019) acs.chemmater.9b00450. https://doi.org/10.1021/acs.chemmater.9b00450.
[61] R. Schlaf, P.G. Schroeder, M.W. Nelson, B.A. Parkinson, C.D. Meritt, L.A. Crisafulli, H. Murata, Z.H. Kakafi, Determination of interface dipole and band bending at the Ag/tris (8-hydroxyquinolinato) gallium organic Schottky contact by ultraviolet photoemission spectroscopy, Surface Science. 450 (2000) 142–152. https://doi.org/10.1016/S0039-6028(00)00232-6.
[62] X. Li, Z. Zhang, V.E. Henrich, Inelastic electron background function for ultraviolet photoelectron spectra, Journal of Electron Spectroscopy and Related Phenomena. 63 (1993) 253–265. https://doi.org/10.1016/0368-2048(93)87007-M.
[63] G. Kortüm, W. Braun, G. Herzog, Principles and Techniques of Diffuse-Reflectance Spectroscopy, Angewandte Chemie International Edition. 2 (1963) 333–341.
[64] J. Tauc, R. Grigorovici, A. Vancu, Optical properties and electronic structure of amorphous germanium, Physica Status Solidi (b). 15 (1966) 627–637. https://doi.org/10.1002/pssb.19660150224.
[65] S.E. Braslavsky, A.M. Braun, A.E. Cassano, A.V. Emeline, M.I. Litter, L. Palmisano, V.N. Parmon, N. Serpone, Glossary of terms used in photocatalysis and radiation catalysis (IUPAC Recommendations 2011), Pure and Applied Chemistry. 83 (2011) 931–1014. https://doi.org/10.1351/PAC-REC-09-09-36.
[66] P. Mitchell, C. Scott, J.-P. Bonnelle, J. Grimblot, Ru/Alumina and Ru-Mo/Alumina Catalysts: An XPS Study, Journal of Catalysis. 107 (1987) 482–489. https://doi.org/10.1016/0021-9517(87)90312-5.
[67] J.A. De Los Reyes, S. Göbölös, M. Vrinat, M. Breysse, Preparation and characterization of highly active ruthenium sulphide supported catalysts, Catalysis Letters. 5 (1990) 17–24. https://doi.org/10.1007/BF00772089.
[68] C. Geantet, C. Calais, M. Lacroix, Modèle géométrique de catalyseurs sulfures de type pyrite, Compte Rendu de l'Académie Des Sciences de Paris. 315 (1992) 439–444.
[69] I. Ait-Ichou, M. Formenti, B. Pommier, S.J. Teichner, Photocatalytic Dehydrogenation of Isopropanol on Pt/TiO_2 Catalysts, Journal of Catalysis. 91 (1985) 293–307. https://doi.org/10.1016/0021-9517(85)90343-4.
[70] S.I. Nikitenko, T. Chave, C. Cau, H.-P. Brau, V. Flaud, Photothermal Hydrogen Production Using Noble-Metal-Free $Ti@TiO_2$ Core–Shell Nanoparticles under Visible–NIR Light Irradiation, ACS Catal. 5 (2015) 4790–4795. https://doi.org/10.1021/acscatal.5b01401.
[71] S.L. Kollmannsberger, C.A. Walenta, C. Courtois, M. Tschurl, U. Heiz, Thermal control of selectivity in photocatalytic, water-free alcohol photo-reforming, ACS Catalysis. (2018). https://doi.org/10.1021/acscatal.8b03479.
[72] F. Parrino, P. Conte, C. De Pasquale, V.A. Laudicina, V. Loddo, L. Palmisano, Influence of Adsorbed Water on the Activation Energy of Model Photocatalytic Reactions, The Journal of Physical Chemistry C. 121 (2017) 2258–2267. https://doi.org/10.1021/acs.jpcc.6b11945.
[73] W. Turek, A. Krowiak, Evaluation of oxide catalysts' properties based on isopropyl alcohol conversion, Applied Catalysis A: General. 417–418 (2012) 102–110. https://doi.org/10.1016/j.apcata.2011.12.030.

[74] H. Kisch, D. Bahnemann, Best Practice in Photocatalysis: Comparing Rates or Apparent Quantum Yields?, The Journal of Physical Chemistry Letters. 6 (2015) 1907–1910. https://doi.org/10.1021/acs.jpclett.5b00521.
[75] K. Takanabe, Addressing fundamental experimental aspects of photocatalysis studies, Journal of Catalysis. 370 (2019) 480–484. https://doi.org/10.1016/j.jcat.2018.10.006.
[76] E. Vulliet, J.-M. Chovelon, C. Guillard, J.-M. Herrmann, Factors influencing the photocatalytic degradation of sulfonylurea herbicides by TiO_2 aqueous suspension, Journal of Photochemistry and Photobiology A: Chemistry. 159 (2003) 71–79. https://doi.org/10.1016/S1010-6030(03)00108-4.
[77] G. Dahi, A. Eskandari, J. Dauchet, F. Gros, M. Roudet, J.-F. Cornet, A novel experimental bench dedicated to the accurate radiative analysis of photoreactors: The case study of CdS catalyzed hydrogen production from sacrificial donors, Chemical Engineering and Processing: Process Intensification. 98 (2015) 174–186. https://doi.org/10.1016/j.cep.2015.09.015.
[78] P. Afanasiev, MoS_2 "inorganic fullerenes" combined with TiO_2 in water-methanol suspensions: Highly active hydrogen production photo catalysts operating via transfer of accumulated electrons, International Journal of Hydrogen Energy. 45 (2020) 14696–14712. https://doi.org/10.1016/j.ijhydene.2020.03.191.
[79] U. Diebold, The surface science of titanium dioxide, Surface Science Reports. 48 (2003) 53–229. https://doi.org/10.1016/S0167-5729(02)00100-0.
[80] M. Wang, Q. Liu, N. Xu, N. Su, X. Wang, W. Su, An amorphous CoS_x modified $Mn_{0.5}Cd_{0.5}S$ solid solution with enhanced visible-light photocatalytic H_2-production activity, Catalysis Science & Technology. 8 (2018) 4122–4128. https://doi.org/10.1039/C8CY01253A.
[81] X. Zong, H. Yan, G. Wu, G. Ma, F. Wen, L. Wang, C. Li, Enhancement of Photocatalytic H_2 Evolution on CdS by Loading MoS_2 as Cocatalyst under Visible Light Irradiation, Journal of the American Chemical Society. 130 (2008) 7176–7177. https://doi.org/10.1021/ja8007825.
[82] M. Shao, Y. Shao, S. Ding, J. Wang, J. Xu, Y. Qu, X. Zhong, X. Chen, W.F. Ip, N. Wang, B. Xu, X. Shi, X. Wang, H. Pan, Vanadium disulfide decorated graphitic carbon nitride for super-efficient solar-driven hydrogen evolution, Applied Catalysis B: Environmental. 237 (2018) 295–301. https://doi.org/10.1016/j.apcatb.2018.05.084.
[83] A. Mills, M. Bingham, C. O'Rourke, M. Bowker, Modelled kinetics of the rate of hydrogen evolution as a function of metal catalyst loading in the photocatalysed reforming of methanol by Pt (or Pd)/TiO2, Journal of Photochemistry and Photobiology A: Chemistry. 373 (2019) 122–130. https://doi.org/10.1016/j.jphotochem.2018.12.039.
[84] J. Tang, J.R. Durrant, D.R. Klug, Mechanism of Photocatalytic Water Splitting in TiO_2. Reaction of Water with Photoholes, Importance of Charge Carrier Dynamics, and Evidence for Four-Hole Chemistry, Journal of the American Chemical Society. 130 (2008) 13885–13891. https://doi.org/10.1021/ja8034637.
[85] K.T. Dembele, G.S. Selopal, R. Milan, C. Trudeau, D. Benetti, A. Soudi, M.M. Natile, G. Sberveglieri, S. Cloutier, I. Concina, F. Rosei, A. Vomiero, Graphene below the percolation threshold in TiO_2 for dye-sensitized solar cells, J. Mater. Chem. A. 3 (2015) 2580–2588. https://doi.org/10.1039/C4TA04395B.
[86] Y.-S. Huang, Y.-F. Chen, Electronic-structure study of RuS_2, Physical Review B. 38 (1988) 7997–8001. https://doi.org/10.1103/PhysRevB.38.7997.
[87] S. Brunken, A. Kratzig, P. Bogdanoff, S. Fiechter, K. Ellmer, Structural, optical and electrical properties of $RuS_{2\pm x}$ films, prepared by reactive magnetron sputtering, Thin Solid Films. 527 (2013) 16–20. https://doi.org/10.1016/j.tsf.2012.12.037.
[88] P. Bogdanoff, C. Zachäus, S. Brunken, A. Kratzig, K. Ellmer, S. Fiechter, Ruthenium sulphide thin layers as catalysts for the electrooxidation of water, Phys. Chem. Chem. Phys. 15 (2013) 1452–1459. https://doi.org/10.1039/C2CP42348K.
[89] Z. Nie, R. Long, L. Sun, C.-C. Huang, J. Zhang, Q. Xiong, D.W. Hewak, Z. Shen, O.V. Prezhdo, Z.-H. Loh, Ultrafast Carrier Thermalization and Cooling Dynamics in Few-Layer MoS_2, ACS Nano. 8 (2014) 10931–10940. https://doi.org/10.1021/nn504760x.

[90] D. Friedmann, C. Mendive, D. Bahnemann, TiO_2 for water treatment: Parameters affecting the kinetics and mechanisms of photocatalysis, Applied Catalysis B: Environmental. 99 (2010) 398–406. https://doi.org/10.1016/j.apcatb.2010.05.014.
[91] P. Singhal, H.N. Ghosh, Hot Charge Carriers in Quantum Dots: Generation, Relaxation, Extraction, and Applications, ChemNanoMat. 5 (2019) 985–999. https://doi.org/10.1002/cnma.201900025.
[92] L.A. King, W. Zhao, M. Chhowalla, D.J. Riley, G. Eda, Photoelectrochemical properties of chemically exfoliated MoS_2, J. Mater. Chem. A. 1 (2013) 8935. https://doi.org/10.1039/c3ta11633f.
[93] B. Behaghel, R. Tamaki, H.-L. Chen, P. Rale, L. Lombez, Y. Shoji, A. Delamarre, A. Cattoni, S. Collin, Y. Okada, J.-F. Guillemoles, A hot-carrier assisted InAs/AlGaAs quantum-dot intermediate-band solar cell, Semicond. Sci. Technol. 34 (2019) 084001. https://doi.org/10.1088/1361-6641/ab23d0.